Unconventional Antiferromagnetic Quantum Critical Point in $Ba(Fe_{0.97}Cr_{0.03})_2(As_{1-x}P_x)_2$

Wenliang Zhang,[1,2] Yuan Wei,[1,2] Tao Xie,[1,2] Zhaoyu Liu,[1,2] Dongliang Gong,[1,2] Xiaoyan Ma,[1,2] Ding Hu,[3,4] Petr Čermák,[5,6] Astrid Schneidewind,[5] Gregory Tucker,[7] Siqin Meng,[8,9] Zita Huesges,[8] Zhilun Lu,[8] Jianming Song,[10] Wei Luo,[10] Liangcai Xu,[11] Zengwei Zhu,[11] Xunqing Yin,[12] Hai-Feng Li,[12] Yi-feng Yang,[1,2,13] Huiqian Luo,[1,13] and Shiliang Li[1,2,13,*]

[1]*Beijing National Laboratory for Condensed Matter Physics, Institute of Physics, Chinese Academy of Sciences, Beijing 100190, China*

[2]*School of Physical Sciences, University of Chinese Academy of Sciences, Beijing 100190, China*

[3]*Center for Advanced Quantum Studies and Department of Physics, Beijing Normal University, Beijing 100875, China*

[4]*Department of Physics and Astronomy, Rice University, Houston, Texas 77005, USA*

[5]*Forschungszentrum Jülich GmbH, Jülich Centre for Neutron Science (JCNS) at Heinz Maier-Leibnitz Zentrum (MLZ), Lichtenbergstrasse 1, 85748 Garching, Germany*

[6]*Charles University, Faculty of Mathematics and Physics, Department of Condensed Matter Physics, Ke Karlovu 5, 121 16, Praha, Czech Republic*

[7]*Laboratory for Neutron Scattering, Paul Scherrer Institut, CH-5232 Villigen, Switzerland*

[8]*Helmholtz-Zentrum Berlin für Materialien und Energie GmbH, D-14109 Berlin, Germany*

[9]*China Institute of Atomic Energy, Beijing 102413, China*

[10]*Key Laboratory of Neutron Physics and Institute of Nuclear Physics and Chemistry, China Academy of Engineering Physics, Mianyang 621999, China*

[11]*Wuhan National High Magnetic Field Center and School of Physics, Huazhong University of Science and Technology, Wuhan 430074, China*

[12]*Institute of Applied Physics and Materials Engineering, University of Macau, Avenida da Universidade, Taipa, 999078 Macau, China*

[13]*Songshan Lake Materials Laboratory, Dongguan, Guangdong 523808, China*

(Received 28 March 2018; revised manuscript received 4 October 2018; published 24 January 2019)

We have systematically studied physical properties of $Ba(Fe_{0.97}Cr_{0.03})_2(As_{1-x}P_x)_2$, where superconductivity in $BaFe_2(As_{1-x}P_x)_2$ is fully suppressed by just 3% of Cr substitution of Fe. A quantum critical point is revealed at $x \sim 0.42$, where non-Fermi-liquid behaviors similar to those in $BaFe_2(As_{1-x}P_x)_2$ are observed. Neutron diffraction and inelastic neutron scattering measurements suggest that the quantum critical point is associated with the antiferromagnetic order, which is not of conventional spin-density-wave type as evidenced by the ω/T scaling of spin excitations. On the other hand, no divergence of low-temperature nematic susceptibility is observed when x is decreased to 0.42 from higher doping level, demonstrating that there are no nematic quantum critical fluctuations. Our results suggest that non-Fermi-liquid behaviors in iron-based superconductors can be solely resulted from the antiferromagnetic quantum critical fluctuations, which cast doubts on the role of nematic fluctuations played in the normal-state properties in iron-based superconductors.

DOI: 10.1103/PhysRevLett.122.037001

An antiferromagnetic (AFM) order may be continuously driven to zero by a nonthermal control parameter, resulting in a quantum critical point (QCP) and non-Fermi-liquid (NFL) behaviors in the itinerant electron systems [1]. In iron-based superconductors, it has been shown that the AFM order disappears around the optimal doping level in many systems [2], suggesting the presence of AFM QCPs and their importance in understanding the unconventional superconductivity. An electronic nematic phase that breaks the in plane C_4 rotational symmetry is also closely accompanied with the collinear AFM order in iron-based superconductors [3]. Nematic QCPs are thus suggested to present [4–6] and could give rise to NFL behaviors [7,8]. The question arises as to which kind of quantum critical fluctuations is more significant in affecting the normal-state properties of iron-based superconductors. However, both QCPs typically happen around optimal doping level, where superconductivity always takes place at finite temperature and precludes detailed studies on them.

Among different families of iron-based superconductors, $BaFe_2(As_{1-x}P_x)_2$ (BFAP) is the most promising system that shows many exotic properties, which are thought to result from a QCP lying beneath the superconducting dome [9], including, but not limited to, linear temperature dependence

of resistivity, enhancement of effective electron mass, and scaling behaviors [10–15]. Both the AFM and nematic QCPs are suggested to present around the optimal doping level [4,16]. Even when the AFM order disappears in a weakly first-order fashion [17,18], magnetic quantum critical fluctuations may still present [19]. While the superconductivity may be completely suppressed by the magnetic field [14,15], the limited probes make it hard to further understand the nature of the QCP.

In this Letter, we use Cr doping as a way to suppress superconductivity without significantly disturbing the long-range AFM order [20,21], which enables us to study the nature of the QCP at very low temperature. It is found that just 3% of Cr substitution of Fe can fully suppress superconductivity in BFAP and reveal a quantum phase transition at $x \sim 0.42$. The linear temperature dependence of resistivity in BFAP, which is the signature of NFL behaviors, can be still clearly observed in Cr-BFAP. While both the AFM and nematic orders disappear at this doping, only the AFM quantum critical point is found. Our results show that NFL behaviors in iron-based superconductors can solely result from the AFM quantum critical fluctuations, which are *not* of conventional spin-density-wave type as evidenced by the ω/T scaling of spin excitations.

The $Ba(Fe_{0.97}Cr_{0.03})_2(As_{1-x}P_x)_2$ (Cr-BFAP) single crystals were grown using a Ba_2As_3/Ba_2P_3 self-flux method as described previously [18], and the chemical compositions are determined by inductively coupled plasma analysis. The resistance and heat capacity were measured on the physical property measurement system (PPMS, Quantum Design). The nematic susceptibility is also measured on the PPMS with a homemade uniaxial pressure device based on a piezobender [5,22]. The magnetoresistance was measured at Wuhan National High Magnetic Field Center, China. Neutron diffraction experiments were carried out at the TASP triple-axis spectrometer (TAS) at Paul Scherrer Institute, Switzerland, V2 TAS at Helmholtz-Zentrum Berlin für Materialien und Energie, Germany, Kunpeng TAS at Key Laboratory of Neutron Physics and Institute of Nuclear Physics and Chemistry, China, and Bamboo TAS at China Institute of Atomic Energy, China. The inelastic neutron scattering experiment was carried out at PANDA TAS at MLZ, Germany, with E_f fixed at 5.1 meV [23]. About 140 single crystals were coaligned with a total mass of about 1.7 g resulting in the single Bragg peak with full width at half maximum of about 1.5°. We use the tetragonal notation, and the scattering plane is (H, H, L) for all the neutron scattering experiments.

Figure 1(a) shows the temperature dependence of normalized resistivity $R_N = R(T)/R(300\ \mathrm{K})$ in Cr-BFAP, where no sign of superconductivity exists. Interestingly, R_N in the $x = 0.42$ sample has a roughly linear temperature dependence down to 2 K, which has always been treated as a typical NFL behavior. Accordingly, the Cr-BFAP system can be divided into two regimes. For the $x < 0.42$ samples,

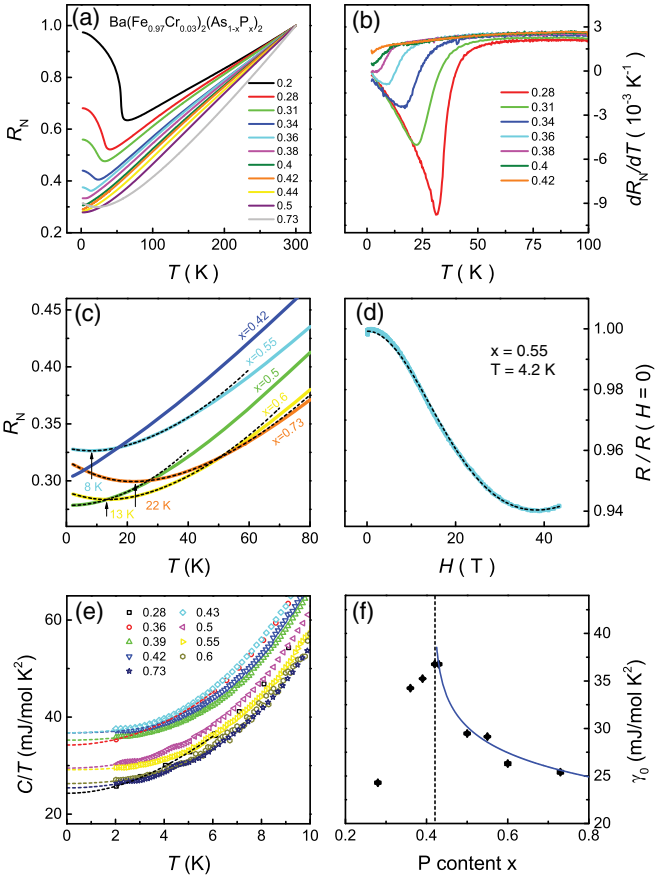

FIG. 1. (a) Temperature dependence of R_N in $Ba(Fe_{0.97}Cr_{0.03})_2(As_{1-x}P_x)_2$. (b) Temperature dependence of $d(R_N)/dT$. (c) Low-temperature R_N for the $x \geq 0.42$ samples. The dashed solid lines show fitting results as described in the main text. The arrows indicate T_{min} where R_N is minimum. (d) Field dependence of resistivity for the $x = 0.55$ sample at 6 K. The dashed line is the fitted result as described in the main text. (e) Specific heat results plotted as C/T vs T. The dashed lines are fitted results as described in the main text. (f) Doping dependence of γ_0. The error bars are from the fittings. The solid line is fitted as $D\ \ln(x - x_c) + y_0$, where both D and y_0 are constants, and $x_c = 0.42$.

both the AFM and nematic transitions present, which is shown by the sharp increase of R_N at low temperature [20]. Figure 1(b) further gives the temperature dependence of $d(R_N)/dT$, where the single dips suggest that the AFM and nematic transitions always happen at the same temperature as in the underdoped BFAP, i.e., $T_N = T_s$ [17,18].

In overdoped samples ($x > 0.42$), $R_N(T)$ deviates from the linear-T behavior below certain temperatures and shows a slight upturn at lower temperature, as shown in Fig. 1(c). In overdoped BFAP, the resistivity shows T^2 behavior at low temperature when superconductivity is completely suppressed by a high magnetic field [14]. Here we fit the low-temperature resistance by $R = R_0 + AT^2 + R_K$ [Fig. 1(c)], where R_0 and A are temperature-independent constants. R_K takes the form of Kondo scattering and is

described as $B\{1-\ln(T/T_K)/[(\ln T/T_K)^2+C]^{1/2}\}$, where B and C are constants, and T_K is the Kondo temperature [24]. Figure 1(d) shows the magnetoresistance of the $x = 0.55$ sample at 4.2 K, which can also be fitted by an empirical function for the Kondo effect [25], i.e., $R(H) = R_0 + R_K[1 - B_s(x)^2] + bH^2$, where R_0, R_K, $B_s(x)$, and bH^2 are the resistance at zero field, the Kondo part of the resistance, the Brillouin function, and the normal magnetoresistance, respectively. Here $x = g\mu_B SH/[K_B(T + T_K)]$, where S and T_K are the magnetic moment and Kondo temperature, respectively. We note that the above analysis includes many parameters that may result in overfitting the data, but the Kondo effect can at least qualitatively describe the low-temperature upturn, which suggests the presence of T^2 dependence of the resistivity at low temperature in overdoped samples after subtracting the contribution from Kondo scattering.

Figure 1(e) shows the results of the specific heat in Cr-BFAP, which can be all fitted as $C/T = \gamma_0 + \beta T^2 + \delta T^4$ for $T < 6$ K [26]. The quadratic and fourth-power terms come from phonon and magnon contributions. In a normal metal, γ_0 is associated with density of states and effective mass. Figure 1(f) shows the doping dependence of γ_0, which increases dramatically around $x = 0.42$ and can be described as logarithmically diverging when approaching $x = 0.42$ from a higher doping level [14]. The ratio between the maximum and minimum values is about 1.5, smaller than the enhancement of effective mass ($\approx$2) in BFAP obtained by quantum oscillation measurements [12]. In the above analysis, we have assumed a linear temperature dependence of the electronic specific heat, which may not be valid near the QCP. However, this will not alter the conclusion that γ_0 shows a significant enhancement around $x = 0.42$.

The above results suggest that a QCP may present around $x = 0.42$. To see whether it is associated with the AFM order, we carried out neutron diffraction experiments on Cr-BFAP. Figure 2(a) shows the Q scans at $L = 3$ for the $x = 0.4$ sample. The appearance of a peak at (0.5, 0.5, 3) at 2 K demonstrates the presence of the collinear AFM order [18]. The sharp peak corresponds to a correlation length larger than 200 Å, suggesting that the AFM order in Cr-BFAP is always long range as in BFAP [18]. Moreover, the AFM moment M linearly goes to zero at about 0.42, as shown in Fig. 2(b). On the other hand, M drops quickly before the AFM order disappears at $x = 0.3$ in BFAP, which has been treated as resulting from a weakly first-order transition [18]. Figures 2(c) and 2(d) show the temperature dependence of M^2, where T_N can be obtained.

The AFM nature of the QCP is also studied by measuring spin excitations in the $x \sim 0.41$ sample with $T_N < 2$ K. Figure 2(e) shows HH scans at 0.3 meV. The peak intensities $S(Q_{\mathrm{AFM}}, \omega)$ at different energies are thus obtained by subtracting the average value of the counts at (0.4, 0.4, 3) and (0.6, 0.6, 3) from that at

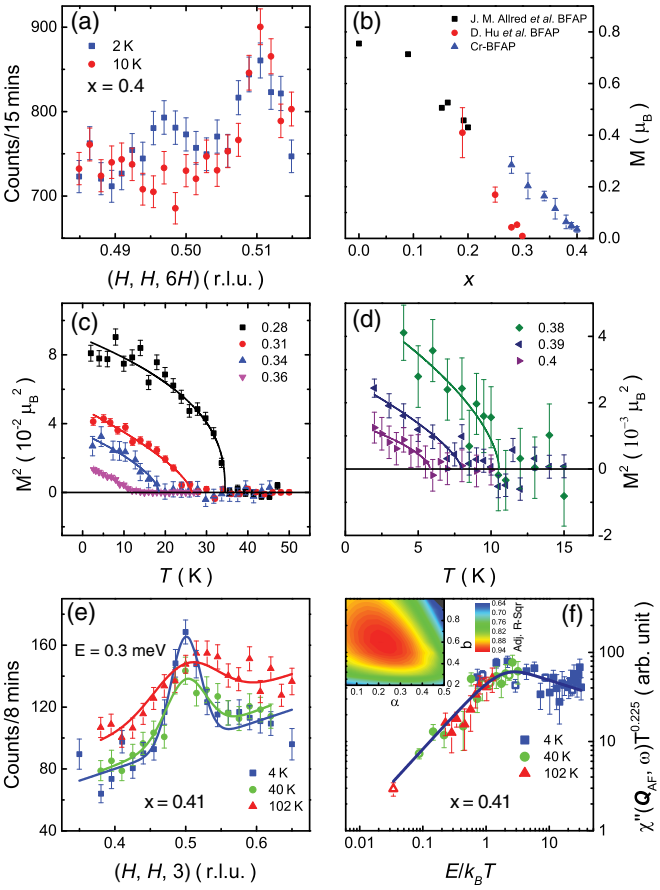

FIG. 2. (a) θ–2θ scans for the $x = 0.4$ Cr-BFAP sample at 2 and 10 K, which correspond to $(H, H, 6H)$ scans within the scattering plane. The right peak is a spurious peak, which shows no temperature dependence. (b) Doping dependence of magnetic moment M. The black squares and red circles are from Refs. [16,17], respectively. (c),(d) Temperature dependence of M^2. The sold lines are fitted as proportional to $(1 - T/T_N)^{2\beta}$. (e) Constant-E scans along $(H, H, 3)$ at 0.3 meV and several temperatures for the $x = 0.41$ Cr-BFAP. The solid lines are fitted results by the Gaussian function with a linear background. (f) ω/T scaling of spin excitations in the $x = 0.41$ Cr-BFAP. The open and solid symbols represent data obtained from constant-E and constant-Q scans, respectively. The solid line is fitted as $\chi''(Q_{QF}, \omega)T^{\alpha} = (k_B T/E)^{\alpha} \tanh(bE/k_B T)$ [27] with $\alpha = 0.225$ and $b = 0.6$. (Inset) Adjusted R^2 of the fitting, where the values of α and b are determined by the maximum value of R^2.

$Q_{\mathrm{AFM}} = (0.5, 0.5, 3)$. Accordingly, the imaginary part of dynamic susceptibility $\chi''(Q_{\mathrm{AFM}}, \omega)$ is calculated as $S(Q_{\mathrm{AFM}}, \omega) \times [1 - \exp(-\hbar\omega/k_B T)]$. The scaling behavior can be found if we plot them as $\chi''(Q_{\mathrm{AFM}}, \omega)T^{0.225} \sim E/k_B T$ [Fig. 2(f)], which suggests the presence of an AFM QCP.

To see whether there is also a nematic QCP, we studied the nematic susceptibility by measuring the elastoresistivity under uniaxial pressure along the tetragonal [110] direction [5,22]. As reported previously, we define ζ as $d(\Delta R/R_0)/dp$, where R_0 is the resistance at zero pressure

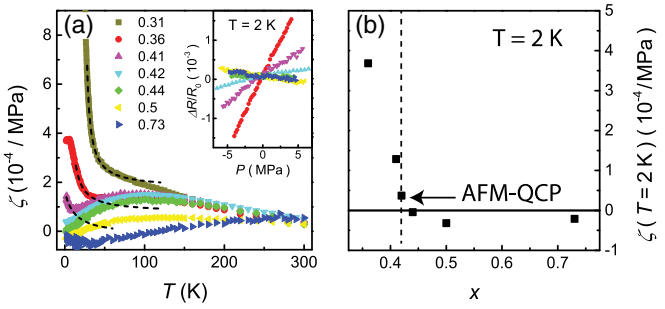

FIG. 3. (a) Temperature dependence of ζ, which is associated with nematic susceptibility as discussed in the main text. The dashed lines are fitted results by a Curie-Weiss-like function near the AFM phase transition. (Inset) Pressure dependence of $\Delta R/R_0$ at 2 K. (b) Doping dependence of ζ at 2 K. The vertical dashed line indicates the position of the QCP at $x \sim 0.42$.

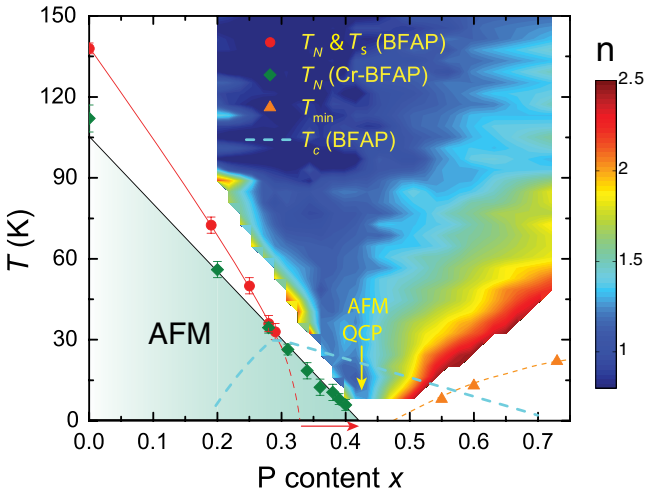

FIG. 4. Phase diagram of the Cr-BFAP system with Cr doping level as 0.03. The diamonds and upper triangles represent $T_N(T_s)$ and $T_{\min}$ of Cr-BFAP. The circles and blue dashed line are T_N and T_c of BFAP [18]. The solid and dashed lines associated with these values are guides to the eye. The color map shows doping and temperature dependence of n, which is obtained by fitting the resistivity as proportional to T^n. The red arrow suggests the move of the QCP from $x \sim 0.33$ in BFAP to $x \sim 0.42$ in Cr-BFAP. While both the AFM and nematic orders present in the lower doping regime, only the AFM QCP exists in Cr-BFAP.

and $\Delta R = R(p) - R(0)$ [5]. Figure 3(a) shows the temperature dependence of ζ, where a broad hump around 100 K is observed in many samples. This is most likely due to the effect of Cr dopants, which may give rise to impurity scattering that is not coupled to nematic fluctuations. Therefore, ζ will be underestimated because of the enhancement of total resistivity and is not a good approximation to nematic susceptibility anymore. However, this effect will not remove the divergent behavior of nematic susceptibility when approaching to the nematic transition, as demonstrated by the upturns at low temperature for $x < 0.42$. These upturns can be roughly fitted by a Curie-Weiss-like function, $\zeta = A/(T - T') + y_0$, as done in other systems [5,22]. The values of A show little change with doping and are about 0.002 K/MPa from $x = 0.31$ to 0.41. Compared to that in optimally doped BFAP [22], A in Cr-BFAP is much smaller, suggesting strong suppression of nematic fluctuations. More importantly, the low-temperature upturn of ζ immediately disappears when x is larger than 0.42 and ζ becomes negative at low temperature. Figure 3(b) shows the doping dependence of ζ at 2 K. It is clear that no divergent behavior of ζ can be found when approaching the QCP at zero temperature from the overdoped side. These results contradict the expectation for the existence of a nematic QCP, which will result in divergent behavior in both the temperature and doping dependence of the nematic susceptibility [4,5,22].

Figure 4 summarizes our results where only the AFM QCP exists although both AFM and nematic transitions present for $x < 0.42$. The color map represents the value of n in fitting the resistivity by $R = R_0 + AT^n$. The NFL behavior of the resistivity is illustrated by the large blue area above the QCP, which corresponds the area dominated by quantum critical fluctuations. For overdoped samples, T^2 behavior of the resistivity appears at low temperature but is covered by the low-temperature upturn [Fig. 1(c)], which presumably comes from Kondo scattering. Compared to the BFAP system [10–15], the position of the QCP in Cr-BFAP shifts from $x \sim 0.33$ to 0.42, and more interestingly, T_N changes linearly with phosphorus doping.

Our results suggest that Cr substitution has significant effects on the properties of BFAP besides the suppression of superconductivity, such as the large increase of residual resistivity, low-temperature upturn of resistivity in overdoped samples, doping dependence of T_N, suppression of nematic fluctuations, and disappearance of nematic QCP. However, Cr substitution seems to have little effect on the nature of the AFM order since the latter remains long range and commensurate. Moreover, the resistivity in overdoped samples shows T^2 dependence as found in BFAP [11,14] after correctly subtracting the contribution from impurity scattering. Interestingly, the low-temperature upturn of the resistivity becomes less and less obvious with decreasing x, which may come from the suppression of the fluctuations of Cr spins by Fe spins near the QCP, or more exotically, the quasiparticles are not well defined anymore around the QCP. Importantly, the sample at the QCP shows the linear temperature dependence of resistivity that is very similar to the optimally doped BFAP [11,14]. Since this kind of behavior has always been treated as one of the major signatures of non-Fermi liquids, we conclude that Cr dopants have insignificant effects on NFL behaviors in BFAP.

The presence of NFL behaviors in Cr-BFAP in the absence of nematic QCP cast doubts on the role played by nematic fluctuations in normal-state properties. In BFAP, divergent nematic susceptibility has been observed around the optimal doping level [4,22], which clearly suggests the presence of nematic QCP in this superconducting system.

However, the disappearance of nematic QCP in Cr-BFAP suggests that quantum nematic fluctuations are not necessary to result in the linear temperature dependence of resistivity. It is thus the AFM quantum fluctuations that dominate the normal-state properties of Cr-BFAP. We note that linear temperature dependence of resistivity is hard to observe in systems where the presence of AFM QCP is in question, such as in $Ba(Fe_{1-x}Co_x)_2As_2$ or $BaFe_{2-x}Ni_xAs_2$, whose AFM orders become short range and glassy around optimal doping level [28–31]. In $FeSe_{1-x}S_x$, where only nematic QCP presents, the temperature dependence of resistivity is not linear [6]. On the other hand, linear temperature dependence of resistivity is found at high pressure in FeSe and $FeSe_{1-x}S_x$ near the boundaries of the pressure-induced AFM order, not at lower pressure where the nematic order disappears [32,33]. Therefore, AFM quantum critical fluctuations may still play a dominate role in resulting NFL behaviors in iron-based superconductors as in many other systems [1].

The ω/T scaling of $\chi''(Q,\omega)$ in Fig. 2(f) suggests that the AFM QCP in Cr-BFAP may be an unconventional QCP [34]. For the conventional spin-density-wave (SDW)-type QCP, the NFL behavior may be understood from the critical scattering of quasiparticles near the hot spots connected by the nesting wave vector of the magnetic order. While the dynamical susceptibility is linear in frequency, there is no ω/T scaling. In heavy-fermion systems, there are fermionic excitations that are no longer well defined near the QCP such that the whole Fermi surface becomes critical, resulting in a local criticality in real space [35] and the ω/T scaling of $\chi''(Q,\omega)$ as shown by theories [35,36] and observed experimentally [27,37]. In our case, although there is a large uncertainty in determining the value of α due to large error bars in raw data [Fig. 2(f)], the ω/T scaling is unambiguous. This type of scaling behavior has also been found in BFAP [38] and electron-doped cuprates [39] with different values of α. This indicates the violation of the conventional SDW scenario and possible involvement of other important low-energy degrees of freedom that may coexist and compete with the long-wavelength spin fluctuations. It should be emphasized that whether the unconventional QCP can be fully applied in our system is still an open question. Revealing the nature of the relevant low-energy bosonic and fermionic excitations might be a crucial step in understanding the pnictide physics in the future.

In conclusion, we have found a unique system of iron pnictides, $Ba(Fe_{0.97}Cr_{0.03})_2(As_{1-x}P_x)_2$, where an AFM QCP presents without nematic quantum critical fluctuations. The observation of the linear temperature dependence of resistivity, one of the most important signatures of non-Fermi liquids, demonstrates that AFM QCP alone is sufficient to give rise to NFL behaviors. Moreover, the AFM QCP is probably the unconventional type, whose underlying mechanism is important for our understanding on the low-energy physics in iron-based superconductors.

This work is supported by the Ministry of Science and Technology of China (No. 2017YFA0302903, No. 2016YFA0300502, No. 2017YFA0303103, No. 2015CB921302, No. 2015CB921303), the National Natural Science Foundation of China (No. 11674406, No. 11874401, No. 11674372, No. 11822411, No. 11774401, No. 11522435), the Strategic Priority Research Program(B) of the Chinese Academy of Sciences (XDB07020300, XDB07020200, XDB25000000), and Key Laboratory of Neutron Physics (NPL), CAEP (No. 2015AB03). H. L. and Y. Y. are supported by the Youth Innovation Promotion Association of CAS. S. L. thanks helpful discussions with Professor Q. Si and Professor R. M. Fernandes.

*slli@iphy.ac.cn

[1] H. v. Löhneysen, A. Rosch, M. Vojta, and P. Wölfle, Rev. Mod. Phys. **79**, 1015 (2007).
[2] P. Dai, Rev. Mod. Phys. **87**, 855 (2015).
[3] R. M. Fernandes, A. V. Chubukov, and J. Schmalian, Nat. Phys. **10**, 97 (2014).
[4] H.-H. Kuo, J.-H. Chu, J. C. Palmstrom, S. A. Kivelson, and I. R. Fisher, Science **352**, 958 (2016).
[5] Z. Liu, Y. Gu, W. Zhang, D. Gong, W. Zhang, T. Xie, X. Lu, X. Ma, X. Zhang, R. Zhang *et al.*, Phys. Rev. Lett. **117**, 157002 (2016).
[6] S. Hosoi, K. Matsuura, K. Ishida, H. Wang, Y. Mizukami, T. Watashige, S. Kasahara, Y. Matsuda, and T. Shibauchi, Proc. Natl. Acad. Sci. U.S.A. **113**, 8139 (2016).
[7] S. A. Hartnoll, R. Mahajan, M. Punk, and S. Sachdev, Phys. Rev. B **89**, 155130 (2014).
[8] S. Lederer, Y. Schattner, E. Berg, and S. A. Kivelson, Proc. Natl. Acad. Sci. U.S.A. **114**, 4905 (2017).
[9] T. Shibauchi, A. Carrington, and Y. Matsuda, Annu. Rev. Condens. Matter Phys. **5**, 113 (2014).
[10] S. Jiang, H. Xing, G. Xuan, C. Wang, Z. Ren, C. Feng, J. Dai, Z. Xu, and G. Cao, J. Phys. Condens. Matter **21**, 382203 (2009).
[11] S. Kasahara, T. Shibauchi, K. Hashimoto, K. Ikada, S. Tonegawa, R. Okazaki, H. Shishido, H. Ikeda, H. Takeya, K. Hirata *et al.*, Phys. Rev. B **81**, 184519 (2010).
[12] H. Shishido, A. F. Bangura, A. I. Coldea, S. Tonegawa, K. Hashimoto, S. Kasahara, P. M. C. Rourke, H. Ikeda, T. Terashima, R. Settai *et al.*, Phys. Rev. Lett. **104**, 057008 (2010).
[13] K. Hashimoto, K. Cho, T. Shibauchi, S. Kasahara, Y. Mizukami, R. Katsumata, Y. Tsuruhara, T. Terashima, H. Ikeda, M. A. Tanatar *et al.*, Science **336**, 1554 (2012).
[14] J. G. Analytis, H.-H. Kuo, R. D. McDonald, M. Wartenbe, P. M. C. Rourke, N. E. Hussey, and I. R. Fisher, Nat. Phys. **10**, 194 (2014).
[15] I. M. Hayes, R. D. McDonald, N. P. Breznay, T. Helm, P. J. W. Moll, M. Wartenbe, A. Shekhter, and J. G. Analytis, Nat. Phys. **12**, 916 (2016).
[16] Y. Nakai, T. Iye, S. Kitagawa, K. Ishida, H. Ikeda, S. Kasahara, H. Shishido, T. Shibauchi, Y. Matsuda, and T. Terashima, Phys. Rev. Lett. **105**, 107003 (2010).

[17] J. M. Allred, K. M. Taddei, D. E. Bugaris, S. Avci, D. Y. Chung, H. Claus, C. dela Cruz, M. G. Kanatzidis, S. Rosenkranz, R. Osborn *et al.*, Phys. Rev. B **90**, 104513 (2014).
[18] D. Hu, X. Lu, W. Zhang, H. Luo, S. Li, P. Wang, G. Chen, F. Han, S. R. Banjara, A. Sapkota *et al.*, Phys. Rev. Lett. **114**, 157002 (2015).
[19] J. Wu, Q. Si, and E. Abrahams, Phys. Rev. B **93**, 104515 (2016).
[20] R. Zhang, D. Gong, X. Lu, S. Li, P. Dai, and H. Luo, Supercond. Sci. Technol. **27**, 115003 (2014).
[21] R. Zhang, D. Gong, X. Lu, S. Li, M. Laver, C. Niedermayer, S. Danilkin, G. Deng, P. Dai, and H. Luo, Phys. Rev. B **91**, 094506 (2015).
[22] Y. Gu, Z. Liu, T. Xie, W. Zhang, D. Gong, D. Hu, X. Ma, C. Li, L. Zhao, L. Lin *et al.*, Phys. Rev. Lett. **119**, 157001 (2017).
[23] A. Schneidewind and P. Čermák, J. Large-Scale Res. Facil. **1**, A12 (2015).
[24] T. Sugiyama and N. Tsuda, J. Phys. Soc. Jpn. **68**, 1306 (1999).
[25] W. Felsch and K. Winzer, Solid State Commun. **13**, 569 (1973).
[26] Higher-power terms are needed to fit the whole temperature range of the data, but the values of γ_0 will not change.
[27] M. C. Aronson, R. Osborn, R. A. Robinson, J. W. Lynn, R. Chau, C. L. Seaman, and M. B. Maple, Phys. Rev. Lett. **75**, 725 (1995).
[28] D. K. Pratt, M. G. Kim, A. Kreyssig, Y. B. Lee, G. S. Tucker, A. Thaler, W. Tian, J. L. Zarestky, S. L. Bud'ko, P. C. Canfield *et al.*, Phys. Rev. Lett. **106**, 257001 (2011).
[29] H. Luo, R. Zhang, M. Laver, Z. Yamani, M. Wang, X. Lu, M. Wang, Y. Chen, S. Li, S. Chang *et al.*, Phys. Rev. Lett. **108**, 247002 (2012).
[30] A. P. Dioguardi, J. Crocker, A. C. Shockley, C. H. Lin, K. R. Shirer, D. M. Nisson, M. M. Lawson, N. apRoberts Warren, P. C. Canfield, S. L. Bud'ko *et al.*, Phys. Rev. Lett. **111**, 207201 (2013).
[31] X. Lu, D. W. Tam, C. Zhang, H. Luo, M. Wang, R. Zhang, L. W. Harriger, T. Keller, B. Keimer, L.-P. Regnault *et al.*, Phys. Rev. B **90**, 024509 (2014).
[32] J. P. Sun, K. Matsuura, G. Z. Ye, Y. Mizukami, M. Shimozawa, K. Matsubayashi, M. Yamashita, T. Watashige, S. Kasahara, Y. Matsuda *et al.*, Nat. Commun. **7**, 12146 (2016).
[33] K. Matsuura, Y. Mizukami, Y. Arai, Y. Sugimura, N. Maejima, A. Machida, T. Watanuki, T. Fukuda, T. Yajima, Z. Hiroi *et al.*, Nat. Commun. **8**, 1143 (2017).
[34] O. Stockert and F. Steglich, Annu. Rev. Condens. Matter Phys. **2**, 79 (2011).
[35] Q. Si, S. Rabello, K. Ingersent, and J. L. Smith, Nature (London) **413**, 804 (2001).
[36] S. Sachdev, *Quantum Phase Transitions* (Cambridge University Press, Cambridge, England, 1999).
[37] A. Schröder, G. Aeppli, R. Coldea, M. Adams, O. Stockert, H. Löhneysen, E. Bucher, R. Ramazashvili, and P. Coleman, Nature (London) **407**, 351 (2000).
[38] D. Hu, H. Hu, W. Zhang, Y. Wei, S. Li, Y. Gu, X. Ma, D. L. Abernathy, S. Chi, T. J. Williams, Y. Li, Q. Si, and P. Dai, arXiv:1812.11902.
[39] S. D. Wilson, S. Li, P. Dai, W. Bao, J.-H. Chung, H. J. Kang, S.-H. Lee, S. Komiya, Y. Ando, and Q. Si, Phys. Rev. B **74**, 144514 (2006).